Phase diagrams of the Blume-Emery-Griffiths model for semiconducting alloy systems $(ABD_2)_{1-x}(CD)_{2x}$ or $[(AB)_{1-x}C_{2x}]D_2$

Jun Ni* and Shuichi Iwata

Research into Artifacts, Center for Engineering, The University of Tokyo, Kamaba 4-6-1, Meguro-ku, Tokyo 153, Japan
(Received 28 March 1995)

The Blume-Emery-Griffiths model is used to model the ordering of semiconducting alloy systems with chalcopyrite structure and zinc-blende structure as the parents, such as the alloy systems $(ABD_2)_{1-x}(CD)_{2x}$ or $[(AB)_{1-x}C_{2x}]D_2$. The ground states are determined to classify the types of ordering and phase diagrams of the system. The new ordered phases are found at composition $x = \frac{3}{4}$ and $x = \frac{1}{4}$ besides the $x = \frac{1}{2}$ stannite phase for a range of energy parameters. The phase diagrams of the compounds are calculated by the cluster-variation method. Several features of the phase diagrams are discussed and compared with experiment.

I. INTRODUCTION

The ternary ABC_2 chalcopyrite compounds form a large group of semiconducting materials which have important technological interest related to their diverse optical, electrical, and structural properties.[1] Many of these chalcopyrite compounds undergo an order-disorder transition as a function of temperature from chalcopyrite to zinc-blende crystal type.[2,3] Recently chalcopyrite phases have also been found by the growth of ordered ternary III-V semiconductor compounds such as GaAsSb$_2$.[4]

The chalcopyrite structure can be considered as a superlattice of the zinc-blende structure. The ABC_2 chalcopyrite phase possess the tetragonal El_1 structure-type space group $I\bar{4}2d$. In the chalcopyrite structure, two kinds of cations cause the doubling of the unit cell along the c axis and each atom A and B is tetrahedrally coordinated to four atoms C, while each atom C is tetrahedrally coordinated to two atoms A and two atoms B in an ordered manner as shown in Fig. 1. If the cations A and B are distributed at random, the cubic zinc-blende structure would result. Many of these compounds undergo an order-disorder phase transition as a function of temperature to the zinc-blende form due to the thermal disordering of the cation sublattice. When the chalcopyrite compounds are alloyed with II-VI zinc-blende compounds to form alloy system such as $(ABD_2)_{1-x}(CD)_{2x}$ or $(AB)_{1-x}C_{2x}D_2$, the order-disorder transition occurs as a function of composition x.

Recently Newman and Xiang[5] analyzed the phase diagrams of alloys mixing the chalcopyrite crystal structure with the zinc-blende structure using an antiferromagnetic Blume-Emery-Griffiths model for the alloy system as either $(ABD_2)_{1-x}(CD)_{2x}$ or $(AB)_{1-x}C_{2x}D_2$. They demonstrated some of the typical phase diagrams for a range of energy parameters. Some of them show rich structures of ordering transition.

The spin-1 Blume-Emery-Griffiths (BEG) model is a model with a very rich phase diagram.[6-8] The model exhibits a wide variety of transitions of first and second order. The general Hamiltonian of the BEG model that includes only a nearest-neighbor interaction and site energies has the form

$$H = J \sum_{\{i,j\}} s_i s_j - K \sum_{\{i,j\}} s_i^2 s_j^2 + L \sum_{\{i,j\}} (s_i^2 s_j + s_i s_j^2)$$
$$+ \mu \sum_i s_i^2 + h \sum_i s_i, \tag{1}$$

where $\{i,j\}$ indicates a sum over the nearest neigh-
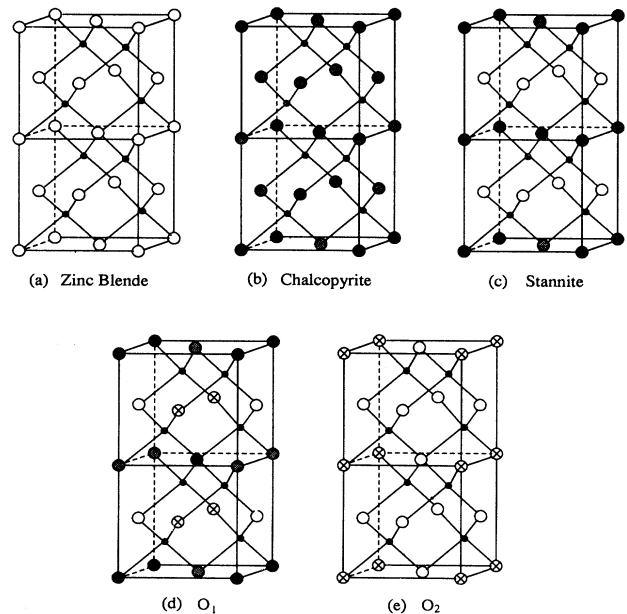
FIG. 1. Representation of ordered phases in $(ABD_2)_{1-x}(CD)_{2x}$ system. (a) A zinc-blende compound CD; (b) a chalcopyrite compound ABD_2; (c) an ordered $x = \frac{1}{2}$ compound, stannite phase; (d) an ordered $x = \frac{3}{4}$ compound O_1; (e) an ordered $x = \frac{1}{4}$ compound O_2. Cations A, B, and C are shown as large solid, hatched, and open circles, respectively, and anions D are shown as the smaller solid circles. The crossed circles in O_1 and O_2 represent $A + B$.

<u>52</u>   3214

bors. The spin-1 Blume-Emery-Griffiths model was originally introduced to describe phase separation and superfluid ordering in ^{3}He-^{4}He mixtures.[6] Later it has been applied to various systems such as multi-component fluids and multicomponent liquid crystal,[9] solid-liquid-gas system,[9] microemulsions,[10] semiconductor alloys,[11,12] and electronic conduction models.[13] Recently a very rich phase diagram was obtained for three-dimensional bipartite lattices by means of a mean field approximation,[14] renormalization-group techniques,[15] and a Monte Carlo renormalization-group calculation.[16] The cluster-variation method has also been used to reveal the rich structures in phase diagrams of the Blume-Emery-Griffiths model on a simple cubic lattice.[17]

In this paper, we have analyzed the ground state diagrams of the alloy system $(ABD_2)_{1-x}(CD)_{2x}$ or $(AB)_{1-x}C_{2x}D_2$ using the Blume-Emery-Griffiths model. According to the phase diagrams of the ground state, we calculated the phase diagrams of the system using the cluster-variation method (CVM) within the energy parameter region $-1 < J/K < 0$ in which the structures of the phase diagrams are rich. This particular region was not covered in Ref. 5. We also compared our results with the experimental phase diagrams for the semiconductor compounds $(CuInTe)_{1-x}(MnTe)_{2x}$ and $(AgInTe)_{1-x}(MnTe)_{2x}$ and explained some of the features of the experimental results.

The outline of this paper is as follows: Section II describes the method used for the calculations. Section III presents the results on the ground states of the system. In Sec. IV the results on the phase diagram calculations are illustrated and discussions of the results and comparisons with experiment are given.

II. METHOD

In the alloy system $(ABD_2)_{1-x}(CD)_{2x}$ or $(AB)_{1-x}C_{2x}D_2$, the atom D always occupies one of two fcc sublattices in the zinc-blende structure and the other sublatttice is shared by atoms A, B, and C. Thus the problem reduces to the ordering of three components (atoms A, B, and C) in the fcc lattice. We can use a BEG Hamiltonian to model the system by mapping the spin $s_i = \{+1, -1, 0\}$ on site $\{i, j\}$ onto the atoms A, B, and C.

If we use $P_{\alpha\beta}$ to represent the pair probability that an atom α and an atom β are nearest-neighbor bonded and represent the nearest-neighbor interaction energies by $E_{\alpha,\beta}$ $[\alpha, \beta = 1(A), 2(B), 3(C)]$, the alloy Hamiltonian of three components with a nearest-neighbor interaction can be written as

$$H_{\text{alloy}} = zN \sum_{\alpha,\beta} E_{\alpha,\beta} P_{\alpha,\beta} - N \sum_\alpha \mu_\alpha x_\alpha, \qquad (2)$$

where $z = 12$ is coordination number, N is the number of the lattice sites, μ_α is chemical potential, and x_α is the composition of the α component.

Using the isomorphism between the BEG Hamiltonian (1) and alloy Hamiltonian (2) of three components,

we can establish the following correspondence between the energy parameter of the BEG Hamiltonian and alloy Hamiltonian:

$$4J = E_{11} + E_{22} - 2E_{12}, \qquad (3)$$

$$4K = -E_{11} - E_{22} - 2E_{12} - 4E_{33} + 4(E_{13} + E_{23}), \qquad (4)$$

$$4L = E_{11} - E_{22} + 2(E_{23} - E_{13}), \qquad (5)$$

$$\mu = \mu_3 - \frac{1}{2}(\mu_1 + \mu_2) - zE_{33} + \frac{z}{2}(E_{13} + E_{23}), \qquad (6)$$

$$h = \frac{1}{2}(\mu_2 - \mu_1) - \frac{z}{2}(E_{23} - E_{13}). \qquad (7)$$

Since the composition of atom A and that of atom B are equal, the number of $s_i = 1$ is equal to the number of $s_i = -1$, which means

$$\sum_i s_i = 0, \qquad \sum_{\{i,j\}}(s_i^2 s_j + s_i s_j^2) = 0. \qquad (8)$$

Therefore, we do not need to consider the parameter L and site energy h. In our problem, there are only two parameters (J and K) and one chemical potential μ which controls the ratio between the composition of atom C and that of atom A or B. The Hamiltonian (1) reduces to the original Blume-Emery-Griffiths Hamiltonian with up-down symmetry[6] used to model tricritical behavior in a ^{3}He-^{4}He mixture,

$$H = J \sum_{\{i,j\}} s_i s_j - K \sum_{\{i,j\}} s_i^2 s_j^2 + \mu \sum_i s_i^2. \qquad (9)$$

We use the tetrahedron cluster-variation method[18,19] to calculate the phase diagrams. Since we consider only nearest-neighbor interactions, we use the nearest-neighbor tetrahedron with vertices on each of the four simple cubic (sc) sublattices of the fcc lattice.

For a fcc lattice of N sites the tetrahedron cluster-variation weight factor is[19]

$$\Omega = \frac{[\prod_{i,j=1}^3 (NP_{ij})!]^6 N!}{[\prod_{i,j,k,l=1}^3 (NP_{ijkl})!]^2 [\prod_{i=1}^3 (NP_i)!]^5}, \qquad (10)$$

where P_i, P_{ij}, and P_{ijkl} are the probabilities of finding the indicated atomic species on a lattice point, on a pair of neighboring sites, and on the vertices of a tetrahedron, respectively, with i, j, k, and l taking values 1, 2, and 3. P_i and P_{ij} are connected with P_{ijkl} by statistical constraints related to the symmetry of phase.

We calculated the phase diagrams by the natural-iteration method with the use of a chemical potential. The procedure is to minimize the grand potential

$$G = E - TS - N \sum_\alpha \mu_\alpha x_\alpha, \qquad (11)$$

where E is the total energy of the system described by the first term of the Hamiltonian (2), T is the temperature,

TABLE I. The eight ground states of the system.

No.	Sublattices (each sc)				Free energy
	I	II	III	IV	
1	$A+B$	$A+B$	$A+B$	$A+B$	$\frac{1}{2}\mu + 6J - \frac{15}{2}K$
2	A	B	A	B	$\frac{1}{2}\mu - 2J - \frac{15}{2}K$
3	$A+B$	$A+B$	$A+B$	C	$\frac{1}{4}\mu + 3J - 3K$
4	$A+B$	$A+B$	C	C	$J + \frac{1}{2}K$
5	$A+B$	C	C	C	$-\frac{1}{4}\mu + 3K$
6	A	B	$A+B$	C	$\frac{1}{4}\mu - J - 3K$
7	A	B	C	C	$-J + \frac{1}{2}K$
8	C	C	C	CE	$-\frac{1}{2}\mu + \frac{9}{2}K$

and the configuration entropy S is given by $S = k_B \ln \Omega$, where k_B is Boltzmann's constant.

The minimization of the grand potential results in a superposition relation used as the basis for natural iteration,

$$P_{ijkl} = \phi(P_{ij}P_{ik}P_{il}P_{jk}P_{jl}P_{kl})^{\frac{1}{2}}(P_iP_jP_kP_l)^{-\frac{5}{8}}, \quad (12)$$

where the factor ϕ depends on the interaction energy and chemical potential

$$\phi = \exp\left[-\frac{\beta}{2}(E_{ij} + E_{ik} + E_{il} + E_{jk} + E_{jl} + E_{kl})\right.$$

$$\left. +\frac{\beta}{8}(\mu_i + \mu_j + \mu_k + \mu_l) + \frac{1}{2}\lambda\beta\right], \quad (13)$$

where $\beta = 1/k_B T$ and λ is a Lagrangian multiplier.

III. GROUND STATES OF THE SYSTEM

We have analyzed the ground states of the system before the calculation of the phase diagrams. Since we consider only nearest-neighbor interactions, we can use the nearest-neighbor tetrahedron with its vertices on each of the four sc lattices to analyze the ground state configurations. The ground states correspond to the configurations of the tetrahedron with the lowest energy. Thus we can obtain the ground states by analysis of the combination of atoms A, B, and C occupying the four vertices of the tetrahedron. Since the composition of atom A and that of atom B are equal, configurations of the tetrahedron with more atoms A than B should be combined with configurations with more atoms B to reflect the up-down symmetry. There are eight types of ground states as is shown in Table I. In Table I, the four vertices are represented as I, II, III, and IV which can also be viewed as four sublattices subdividing the fcc lattice into its four constituent simple cubic lattices. The first type of ground state is the phase separation state with two cluster configuration $AAAA$ and $BBBB$. The second one is the chalcopyrite phase. The third one is the mixed state with compostion $x = 1/4$. Ground states 4 and 5 are also mixed states with composition $x = 1/2$ and $x = 3/4$, respectively. The structure of ground state 5 is shown in Fig. 1. Ground state 6 is the ordered state which is shown in Fig. 1 as

O_1. Ground state 7 is the stannite phase and gound state 8 is the zinc-blende phase.

We have calculated the free energy of the ground states. The phase diagrams of the ground states are drawn by comparing the free energies of these eight types of ground phases, which are shown in Fig. 2 and Fig. 3. Figure 2 corresponds to the case $K > 0$ while Fig. 3 corresponds to the case $K < 0$. The numbers labeling the regions of the interaction parameter in the figures correspond to the labeling numbers of ground states in Table I. From the ground state diagrams, we can classify the phase diagrams as described in the following: When we calculate the phase diagrams, we change the chemical potential μ to scan the whole range of the composition x. The chemical potential can change from $-\infty$ to ∞. The sequence of ground states along the line parallel to the μ axis cooresponds to those of the low-temperature phases in the $T-x$ phase diagram when the chemical potential μ is varied from $-\infty$ to ∞. Thus one may analyze the type of phase diagram according to the sequence of ground states along a line parallel to the μ axis. For $K > 0$, as shown in Fig. 1, there are two types. When $J/K < 0$, from Fig. 1 we can see that ground state 1 (mixed A and B phases) is transformed into ground state 8 (zinc-blende phase) as the normalized chemical potential μ is varied from $-\infty$ to ∞. When $J/K > 0$, ground state 2 (chalcopyrite phase) is transformed into the zinc-blende
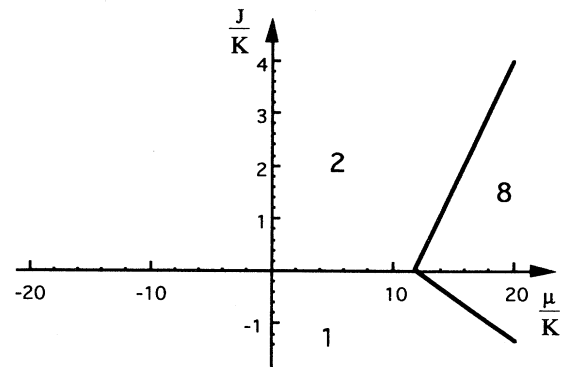
FIG. 2. The phase diagram of ground states of the system with $K > 0$. The numbers refer to the types of ground state in Table I.
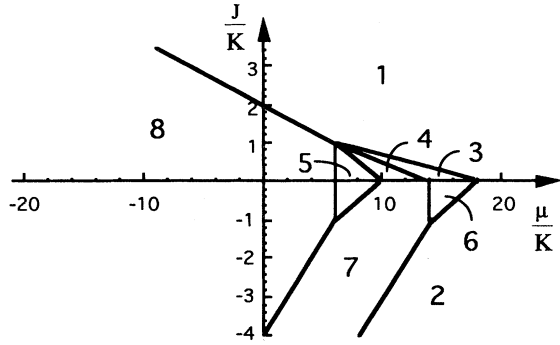
FIG. 3. The phase diagram of ground states of the system with $K < 0$. The numbers refer to the types of ground state in Table I.

phase. For the case of $K < 0$, there are four types of phase diagram which can be seen from Fig. 3. For $J < 0$, there is no chalcopyrite phase. The reason is that the Ising parameter J controls the bonding type between the components A and B. If the components A and B do not phase separate, J should be positive with the Hamiltonian being antiferromagnetic type. So we consider only the case $J > 0$. With $K < 0$, this will be the case $J/K < 0$. There are two types of phase diagram. One with $J/K < -1$ consists of phases 8, 7, and 2 which correspond to chalcopyrite, stannite, and zinc-blende phases, respectively. Another type with $-1 < J/K < 0$ consists of all the five phases shown in Fig. 1.

IV. PHASE DIAGRAMS AND DISCUSSIONS

We have focused our calculations on the regions $-1 < J/K < 0$, in which there are five ground states along the line parallel to the μ axis. As μ changes from $-\infty$ to ∞, one may experience five phases from a chalcopyrite to zinc-blende phase with O_1, stannite phase, and O_2 in between. For the determination of the phase diagrams of the system, we minimize the grand potential G using Kikuchi's natural iteration scheme[18] in which the chemical potential μ and temperature T are the natural variables. As we change the chemical potential μ and temperature T, we can determine the phase boundaries by searching for those special values of the chemical potential μ and corresponding composition x for which two phases coexist.

The configuration of each phase in the phase diagram corresponds to the cluster configuration. Symmetry of each phase is determined by the site probabilities P_i^α. We can also describe the phase by the magnetization and quadrupolar moments of sublattices I, II, III, and IV in the BEG model:

$$m_i = \langle s_i \rangle, \quad q_i = \langle s_i^2 \rangle, \tag{14}$$

where the subscript i represents the four sublattices I, II, III, and IV, and $\langle \cdots \rangle$ indicates a thermodynamic average. The values of these parameters define the following

phases with different symmetry: (1) zinc-blende phase: $m_i = 0$, $q_I = q_{II} = q_{III} = q_{IV}$; (2) chalcopyrite phase: $|m_I| = |m_{II}| = |m_{III}| = |m_{IV}| \neq 0$, $q_I = q_{II} = q_{III} = q_{IV}$; (3) stannite phase: $m_I = -m_{II} \neq 0$, $m_{III} = m_{IV} = 0$, $q_I = q_{II} \neq q_{III} = q_{IV}$; (4) phase O_1: $m_I = -m_{II} \neq 0$, $m_{III} = m_{IV} = 0$, $q_I = q_{II} \neq q_{III} \neq q_{IV}$; (5) phase O_2: $m_i = 0$, $q_I = q_{II} = q_{III} \neq q_{IV}$. There are also some other ordered phases which occur at higher temperature in the phase diagrams such as the phases characterized by $|m_I| = |m_{II}| \neq |m_{III}| = |m_{IV}|$, $q_I = q_{II} \neq q_{III} = q_{IV}$ or $m_i = 0$, $q_I \neq q_{II} \neq q_{III} \neq q_{IV}$.

We have calculated several types of phase diagrams by the cluster-variation method in the parameter region $-1 < J/K < 0$. Figure 4 shows the phase diagrams with $J/K = -0.91$. The value $J/K = -0.91$ is near the boundary line with $J/K = -1$ which divides two regions in the ground state diagram corresponding to different types of the phase diagram (see Fig. 2). $J/K = -1$ represents the pecolation limit of the system, $|J| = |K|$, and so all energies are equal in magnitude to allow pairs of atoms A and B being diluted by atoms C with A, B, and C sitting on a fcc sublattice, as discussed in Ref. 5. From Fig. 4, it can be seen that at high temperature the system undergoes an order-disorder transition from the chalcopyrite phase directly to the zinc-blende phase with the transition being first order. As the temperature decreases, we can see that there is an interim phase C' between the chalcopyrite phase and zinc-blende phase. The transition from the chalcopyrite phase to C' is second order because the order parameter changes continuously. As the temperature decreases, the interim phase changes into another ordered phase with $|m_I| = |m_{II}| \neq |m_{III}| = |m_{IV}|$, $q_I = q_{II} \neq q_{III} = q_{IV}$, and a stannite phase occurs. The transitions from the chalcopyrite phase to phase C'' and that from C'' to the stannite phase are second order. The ordered phases O_1 and O_2 occur at lower temperature. The shaded parts in the figure are the phase separation region. The transition from O_1 to the stannite phase is second order while the transition from the stannite phase to O_2 is first order.
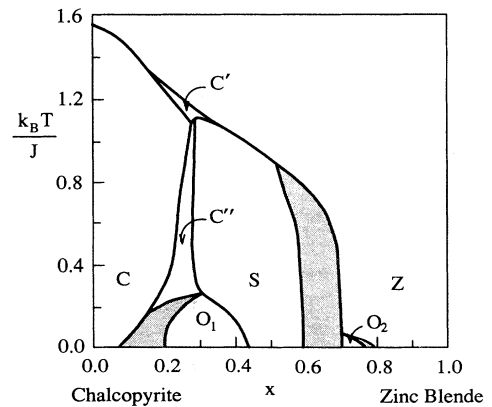
FIG. 4. Phase diagram of the renormalized temperature $k_B T/J$ vs composition x for energies ratio $J/K = -0.91$. Chalcopyrite (C), stannite (S), zinc-blende (Z), O_1, and O_2 phases are indicated.

Figure 5 shows the phase diagram with $J/K = -2/3$. From the figure we can see that the phases O_1 and O_2 occur at a higher temperature than that of Fig. 4. There is also an interim phase. The transition between C'' and O_1 is second order. The transition between phase O_1 and the stannite phase is second order while the transition between the stannite phase and phase O_2 is first order.

Figure 6 shows the phase diagram with parameter $J/K = -0.2$ which is near to another boundary which divides the two types of phase systems of ground states. As we can see from the figure, the upper part of the bulge in the phase diagram is rather flat. The first appeared ordered phase is stannite phase. On top of the O_1 phase there is an interim phase C'' with $m_i = 0$, $q_I = q_{II} = q_{III} \neq q_{IV}$. With a decrease of temperature, phase O_1 and phase O_2 appear. The transition between C'' and O_1 is second order. The transition between phase O_1 and the stannite phase is second order while the transition between the stannite phase and phase O_2 is first order. The transition between the chalcopyrite phase and zinc-blende phase appears at a relatively low temperature.

There are several measurements on the phase diagrams and ordered structures on the system of alloys $(ABD_2)_{1-x}(CD)_{2x}$ or $(AB)_{1-x}C_{2x}D_2$. Aresti et al.[20] have used the differential thermal analysis measurements to obtain the phase diagram of the alloy system $(CuIn)_{1-x}Mn_{2x}Te_2$. They found that manganese tends to order on a stannite type and there is evidence of mixed-symmetry alloys. Quintero et al.[21] obtained more complete phase diagrams of $(CuInTe)_{1-x}(MnTe)_{2x}$ and $(AgInTe)_{1-x}(MnTe)_{2x}$ alloys using differential thermal analysis and x-ray diffraction techniques. MnTe plays the part of a zinc-blende parent with tetrahedral bonding only up to a certain maximum value of composition x_{max} with MnTe itself having a rocksalt structure. The range of compostion investigated was limited to $0 \leq x \leq 0.8$ and the behavior of the MnTe-rich phases was not considered. Their results indicated that there are four struc-
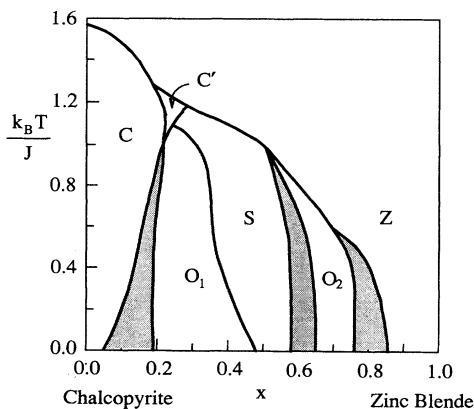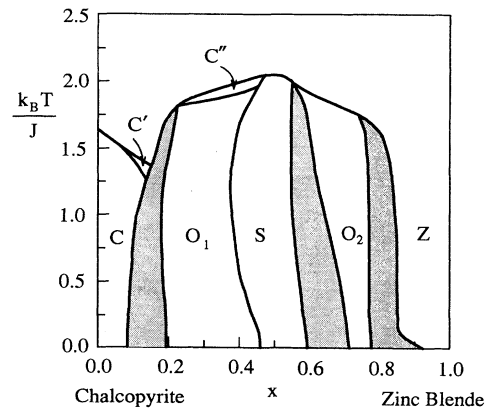
FIG. 6. Phase diagram of the renormalized temperature $k_B T/J$ vs composition x for energies ratio $J/K = -0.2$. Chalcopyrite (C), stannite (S), zinc-blende (Z), O_1, and O_2 phases are indicated.

tures as equilibrium structures: the α phase with chalcopyrite structure, the β phase with zinc-blende structure, the β' phase which they called ordered zinc-blende and believed to be a stannite structure, and the α' phase which they called ordered chalcopyrite and is similiar in some way to the β' phase. Both phase diagrams for $(CuInTe)_{1-x}(MnTe)_{2x}$ and $(AgInTe)_{1-x}(MnTe)_{2x}$ are similiar. They also found that the transition $\beta \to \alpha$ was first order while the transition $\beta' \to \alpha'$ was second order. Their measured phase diagrams are very similiar to our calculated phase diagram Fig. 5. Comparing the location of phases α' and β' in the phase diagram with that of O_1 and the stannite phase and considering that the difference between α and α' and between β and β' was the ordering of manganese on the cation sublattice and that the ordered α' and β' phases have very similiar behavior, we suggest that the ordered α' is O_1 phase and β' phase is the stannite phase. The difference between phase O_1 and the stannite structure is $q_{II} \neq q_{III}$ as described by the order parameters in Eq. (10). The transition between O_1 and the stannite structure is second order which is same as the measurement.

In summary, we have investigated the ordering of the (chalcopyrite–zinc-blende) system using the Blume-Emery-Griffiths model. The ground states are determined and new ordered phases are found. The phase diagrams of the system with parameters in the region $-1 < J/K < 0$ are calculated by the cluster-variation method and rich structures of the phase diagrams are illustrated. We have compared our results with the experimental phase diagrams of the alloy systems $(CuInTe)_{1-x}(MnTe)_{2x}$ and $(AgInTe)_{1-x}(MnTe)_{2x}$.

ACKNOWLEDGMENT

FIG. 5. Phase diagram of the renormalized temperature $k_B T/J$ vs composition x for energies ratio $J/K = -2/3$. Chalcopyrite (C), stannite (S), zinc-blende (Z), O_1, and O_2 phases are indicated.

* Permanent address: Department of Physics, Tsinghua University, Beijing 100084, P. R. China.

[1] J. L. Shay and J. H. Wernick, *Ternary Chalcopyrite Semiconductor: Growth, Electronic Properties and Applications* (Pergamon Press, Oxford, 1975).

[2] L. Garbato, F. Ledda, and A. Rucci, Prog. Cryst. Growth Charact. **15**, 1 (1987).

[3] J. J. M. Brinsma, L. J. Giling, and J. Bloem, Phys. Status Solidi A **63**, 595 (1981).

[4] H. R. Jen, M. J. Cheng, and G. B. Stringfellow, Appl. Phys. Lett. **48**, 1603 (1986); G. B. Stringfellow, J. Cryst. Growth **98**, 1 (1989).

[5] K. E. Newman and X. Xiang, Phys. Rev. B **44**, 4677 (1991).

[6] M. Blume, V. J. Emery, and R. B. Griffiths, Phys. Rev. A **4**, 1071 (1971).

[7] D. Mukamel and M. Blume, Phys. Rev. A **10**, 610 (1974).

[8] A. N. Berker and M. Wortis, Phys. Rev. B **14**, 4946 (1976).

[9] J. Lajzerowicz and J. Sivardière, Phys. Rev. A **11**, 2079 (1975); J. Sivardière and J. Lajzerowicz, *ibid.* **11**, 2090 (1975); **11**, 2101 (1975).

[10] M. Schick and W. H. Shih, Phys. Rev. B **34**, 1797 (1986).

[11] K. E. Newmann and J. D. Dow, Phys. Rev. B **27**, 7495 (1983).

[12] B. L. Gu, J. Ni, and J. L. Zhu, Phys. Rev. B **45**, 4071 (1992).

[13] S. A. Kivelson, V. J. Emery, and H. Q. Lin, Phys. Rev. B **42**, 6523 (1990).

[14] W. Hoston and A. N. Berker, Phys. Rev. Lett. **67**, 1027 (1991).

[15] W. Hoston and A. N. Berker, J. Appl. Phys. **70**, 6101 (1991).

[16] R. R. Netz, Europhys. Lett. **17**, 373 (1992).

[17] A. Rosengren and S. Lapinskas, Phys. Rev. Lett. **71**, 165 (1993).

[18] R. Kikuchi, J. Chem. Phys. **60**, 1071 (1974).

[19] R. Kikuchi, Acta Metall. **25**, 195 (1977); R. Kikuchi, D. de Fontaine, M. Murakami, and T. Nakamura, *ibid.* **25**, 207 (1977).

[20] A. Aresti, L. Garboto, A. Geddo-Lehman, and P. Manca, in *Ternary and Multinary Compounds*, edited by S. K. Deb and A. Zunger (Materials Research Society, Pittsburgh, 1987), p. 497.

[21] M. Quintero, P. Grima, R. Tovar, G. S. Pérez, and J. C. Woodley, Phys. Status Solidi A **107**, 205 (1988).